Proposal for a superconducting photon number resolving detector with large dynamic range

Proposal for a superconducting photon number resolving detector with large dynamic range

Saeedeh Jahanmirinejad* and Andrea Fiore

COBRA Research Institute, Eindhoven University of Technology, P.O. Box 513, 5600 MB Eindhoven, The Netherlands

*s.jahanmiri.nejad@tue.nl

Abstract: We propose a novel photon number resolving detector structure with large dynamic range. It consists of the series connection of *N* superconducting nanowires, each connected in parallel to an integrated resistor. Photon absorption in a wire switches its current to the parallel resistor producing a voltage pulse and the sum of these voltages is measured at the output. The combination of this structure and a high input impedance preamplifier result in linear, high fidelity, and fast photon detection in the range from one to several tens of photons.

OCIS codes: (040.5160) Photodetectors; (040.3780) Low light level.

References and links

1. E. Knill, R. Laflamme, and G. J. Milburn, "A scheme for efficient quantum computation with linear optics," Nature **409**(6816), 46–52 (2001).
2. P. Kok, K. Nemoto, T. C. Ralph, J. P. Dowling, and G. J. Milburn, "Linear optical quantum computing with photonic qubits," Rev. Mod. Phys. **79**(1), 135–174 (2007).
3. N. Sangouard, C. Simon, J. Minář, H. Zbinden, H. de Riedmatten, and N. Gisin, "Long-distance entanglement distribution with single-photon sources," Phys. Rev. A **76**(5), 050301 (2007).
4. M. Fujiwara and M. Sasaki, "Direct measurement of photon number statistics at telecom wavelengths using a charge integration photon detector," Appl. Opt. **46**(16), 3069–3074 (2007).
5. A. E. Lita, A. J. Miller, and S. W. Nam, "Counting near-infrared single-photons with 95% efficiency," Opt. Express **16**(5), 3032–3040 (2008).
6. B. E. Kardynał, Z. L. Yuan, and A. J. Shields, "An avalanche-photodiode-based photon-number-resolving detector," Nat. Photonics **2**(7), 425–428 (2008).
7. J. Kitaygorsky, S. Dorenbos, E. Reiger, R. Schouten, V. Zwiller, and R. Sobolewski, "HEMT-based readout technique for dark- and photon-count studies in NbN superconducting single-photon detectors," IEEE Trans. Appl. Supercond. **19**(3), 346 (2009).
8. M. J. Fitch, B. C. Jacobs, T. B. Pittman, and J. D. Franson, "Photon-number resolution using time-multiplexed single-photon detectors," Phys. Rev. A **68**(4), 043814 (2003).
9. P. Eraerds, E. Pomarico, J. Zhang, B. Sanguinetti, R. Thew, and H. Zbinden, "32 bin near-infrared time-multiplexing detector with attojoule single-shot energy resolution," Rev. Sci. Instrum. **81**(10), 103105 (2010).
10. L. A. Jiang, E. A. Dauler, and J. T. Chang, "Photon-number-resolving detector with 10 bits of resolution," Phys. Rev. A **75**(6), 062325 (2007).
11. E. A. Dauler, A. J. Kerman, B. S. Robinson, J. K. W. Yang, B. Voronov, G. Goltsman, S. A. Hamilton, and K. K. Berggren, "Photon-number-resolution with sub-30-ps timing using multi-element superconducting nanowire single photon detectors," J. Mod. Opt. **56**(2-3), 364–373 (2009).
12. A. Divochiy, F. Marsili, D. Bitauld, A. Gaggero, R. Leoni, F. Mattioli, A. Korneev, V. Seleznev, N. Kaurova, O. Minaeva, G. Gol'tsman, K. G. Lagoudakis, M. Benkhaoul, F. Lévy, and A. Fiore, "Superconducting nanowire photon-number-resolving detector at telecommunication wavelengths," Nat. Photonics **2**(5), 302–306 (2008).
13. F. Marsili, D. Bitauld, A. Gaggero, S. Jahanmirinejad, R. Leoni, F. Mattioli, and A. Fiore, "Physics and application of photon number resolving detectors based on superconducting parallel nanowires," New J. Phys. **11**(4), 045022 (2009).
14. G. Gol'tsman, O. Okunev, G. Chulkova, A. Lipatov, A. Semenov, K. Smirnov, B. Voronov, A. Dzardanov, C. Williams, and R. Sobolewski, "Picosecond superconducting single-photon optical detector," Appl. Phys. Lett. **79**(6), 705 (2001).
15. K. M. Rosfjord, J. K. W. Yang, E. A. Dauler, A. J. Kerman, V. Anant, B. M. Voronov, G. N. Gol'tsman, and K. K. Berggren, "Nanowire single-photon detector with an integrated optical cavity and anti-reflection coating," Opt. Express **14**(2), 527–534 (2006).
16. B. Baek, J. A. Stern, and S. W. Nam, "Superconducting nanowire single-photon detector in an optical cavity for front-side illumination," Appl. Phys. Lett. **95**(19), 191110 (2009).

#157785 - $15.00 USD Received 9 Nov 2011; revised 16 Jan 2012; accepted 7 Feb 2012; published 14 Feb 2012

17. A. Gaggero, S. Jahanmirinejad, F. Marsili, F. Mattioli, R. Leoni, D. Bitauld, D. Sahin, G. J. Hamhuis, R. Nötzel, R. Sanjines, and A. Fiore, "Nanowire superconducting single-photon detectors on GaAs for integrated quantum photonic applications," Appl. Phys. Lett. **97**(15), 151108 (2010).
18. M. G. Tanner, C. M. Natarajan, V. K. Pottapenjara, J. A. O'Connor, R. J. Warburton, R. H. Hadfield, B. Baek, S. Nam, S. N. Dorenbos, E. B. Ureña, T. Zijlstra, T. M. Klapwijk, and V. Zwiller, "Enhanced telecom wavelength single-photon detection with NbTiN superconducting nanowires on oxidized silicon," Appl. Phys. Lett. **96**(22), 221109 (2010).
19. J. P. Sprengers, A. Gaggero, D. Sahin, S. Jahanmirinejad, G. Frucci, F. Mattioli, R. Leoni, J. Beetz, M. Lermer, M. Kamp, S. Höfling, R. Sanjines, and A. Fiore, "Waveguide superconducting single-photon detectors for integrated quantum photonic circuits," Appl. Phys. Lett. **99**(18), 181110 (2011).
20. E. A. Dauler, A. J. Kerman, D. Rosenberg, S. Pan, M. E. Grein, R. J. Molnar, R. E. Correa, M. G. Bawendi, K. K. Berggren, J. D. Moores, and D. M. Boroson, "Superconducting nanowire single photon detectors," in *Proceedings of 24th Annual Meeting of IEEE Photonics Society*, 2011, pp.350–351.
21. W. H. P. Pernice, C. Schuck, O. Minaeva, M. Li, G. N. Goltsman, A. V. Sergienko, and H. X. Tang, "High speed travelling wave single-photon detectors with near-unity quantum efficiency," arXiv:1108.5299, (2011).
22. J. K. W. Yang, A. J. Kerman, E. A. Dauler, V. Anant, K. M. Rosfjord, and K. K. Berggren, "Modeling the electrical and thermal response of superconducting nanowire single-photon detectors," IEEE Trans. Appl. Supercond. **17**(2), 581 (2007).
23. A. J. Kerman, J. K. W. Yang, R. J. Molnar, E. A. Dauler, and K. K. Berggren, "Electrothermal feedback in superconducting nanowire single-photon detectors," Phys. Rev. B **79**(10), 100509 (2009).
24. J. S. Lundeen, A. Feito, H. Coldenstrodt-Ronge, K. L. Pregnell, Ch. Silberhorn, T. C. Ralph, J. Eisert, M. B. Plenio, and I. A. Walmsley, "Tomography of quantum detectors," Nat. Phys. **5**(1), 27–30 (2009).

1. Introduction

Resolving the number of photons in a weak optical pulse is an indispensable requirement for many applications, including linear optics quantum computing [1,2], quantum-key-distribution [3], and high-sensitivity optical communications. However, a suitable technology for fast and sensitive photon-number resolving (PNR) detection is not yet available, particularly in the telecom wavelength range. Indeed, sensitivity at the single photon level is usually achieved by using a very nonlinear internal gain process, which makes the detection response independent of the photon number. Existing approaches to PNR detectors are especially limited in terms of dynamic range, i.e. the maximum number of photons which can be measured, typically in the 1-4 photons range. Here we propose an approach which can provide high fidelity PNR detection from one up to several tens of photons, therefore bridging the gap between single-photon detectors and conventional linear optical detectors.

A first approach to realize PNR detectors consists of combining linear operation and single photon sensitivity in a single detector. In telecom wavelength range, this has been demonstrated in charge integrated photon detectors (CIPDs), which are promising in terms of quantum efficiency (QE) and dynamic range, but suffer from low readout speed (40Hz) [4]. Transition edge sensors (TES's) also show PNR capability, with very high (95%) QE and very low dark-count rates, but have maximum counting rates below 1MHz and also the drawback of a very low (<100mK) operation temperature [5]. InGaAs single photon avalanche detectors (SPADs), in conjunction with self-differencing circuits, are reported to provide photon-number resolution with QE of 10% and repetition rate of 622MHz, but have limited photon-number-discrimination ability, with the requirement of complicated readout circuit [6]. The readout of nanowire superconducting single photon detectors (SSPDs) with a high impedance load has also been proposed to add PNR functionality to these detectors, but produces latching of the detector in a permanent resistive state [7].

The second approach to realize PNR detectors is to temporally or spatially multiplex the incoming beam onto an array of single photon detectors, so that each detector does not receive more than one photon. Time-multiplexing necessarily increases the response time, leading to limited maximum counting rates [8,9]. Space multiplexed InGaAs SPADs are usually plagued by high dark count rate and long dead times [10]. A four-element array of SSPDs, with separate readout for each element, has been demonstrated to count up to 4 photons with sub 30ps timing resolution and 25% system QE at 1550 nm [11], but generally arrays of independent single photon detectors additionally involve separate contacting, amplification

#157785 - $15.00 USD Received 9 Nov 2011; revised 16 Jan 2012; accepted 7 Feb 2012; published 14 Feb 2012

and discrimination and are intrinsically not scalable to larger photon numbers. An alternative scheme is the parallel nanowire detector (PND) that uses an array of superconducting nanowires connected electrically in parallel [12]. The currents from the switching wires are added so that the single output signal is proportional to the number of wires that have fired. A PND, although known as the fastest PNR, has the drawback of leakage current redistribution to the still unfiring sections, which puts a limit on the bias current, (and hence on the QE) as well as to the total number of nanowires in parallel [13].

In this paper we propose a PNR detector based on the series connection of superconducting nanowires, called hereafter Series Nanowire Detector (SND). Like the PND, it is based on spatial multiplexing of SSPDs. The SSPD [14], in brief, is an ultrathin (~4nm thick), narrow (~100nm wide) superconducting wire, arranged in a meander-like geometry to cover a larger area and maximize the probability of photon absorption. It is cooled down typically to 2-4 K to operate in superconducting state and is biased slightly below its critical current. The photon detection process is based on formation of a resistive section in the nanowire upon absorption of an incoming photon, which can be amplified and results in a measurable voltage pulse. SSPDs offer broad spectral response from ultraviolet to infrared wavelengths, high count rate, low dark count rate and small timing jitter. Although low optical absorption in the ultrathin nanowire structures limits QE, it has been reported that by integrating these detectors with advanced optical structures such as optical microcavities or waveguides [15–21] the QE can be enhanced substantially. SNDs preserve all the advantages of SSPDs in terms of simplicity, sensitivity, timing resolution and speed. As shown below, they solve the current redistribution issues related to PNDs, therefore offer a much larger dynamic range from one up to several tens of photons.

2. Device structure

The proposed structure of the SND is made of the series connection of *N* superconducting nanowires, each connected in parallel to a resistor (R_p). As shown in Fig. 1, each nanowire is electrically modeled as an inductor (L_k) in series with a time variable resistor $R_n(t)$ with a nonzero value after absorption of a photon. The parallel resistor R_p may be monolithically integrated with the nanowire, for example as shown in Fig. 1, by deposition and patterning of gold or other metal thin films. The resistor could also be defined below or above the NbN wire, in order to maximize the filling factor.

All the detecting sections are equally biased (in series) with a bias current close to the critical current (typically the same for all branches). Absorption of a photon in one branch temporarily perturbs the superconductivity [14], forming a resistive section across the wire. If the value of R_p is smaller than the photon-induced normal resistance of the nanowire $R_n(t)$, the bias current switches to the parallel resistor and a voltage pulse is formed across the branch. If more branches fire, the voltages produced across them are summed up and the output voltage is proportional to the number of firing detectors, i.e. the number of absorbed photons, provided that all photons are absorbed in distinct branches. The parallel resistance R_p has the key role of discharging the wire after a resistive transition, thus avoiding latching. We note that the SND has an electrical structure which is dual to the one of the PND, where the wires have resistors in series and are connected in parallel.

In the case of the traditional 50Ω readout via a coaxial cable, after one section absorbs the photon, the bias current is partially redistributed to the load, temporarily reducing the bias in the unfiring branches, and therefore introducing a dead time and reducing the output voltage, as it will be shown below. This effect can be minimized by using a preamplifier with large input impedance placed in the cryostat close to the device. A high input impedance cryogenic preamplifier is readily implemented using the metal-semiconductor-field-effect-transistor (MESFET) or high-electron-mobility-transistor (HEMT) technologies. We note that even with the standard 50Ω load, this configuration is preferable to the PND structure in which photon absorption in one section results in the increase of the bias current in the other still

#157785 - $15.00 USD Received 9 Nov 2011; revised 16 Jan 2012; accepted 7 Feb 2012; published 14 Feb 2012

superconducting sections (unfiring), putting a limit on the maximum bias current and hence on the QE and dynamic range [13].

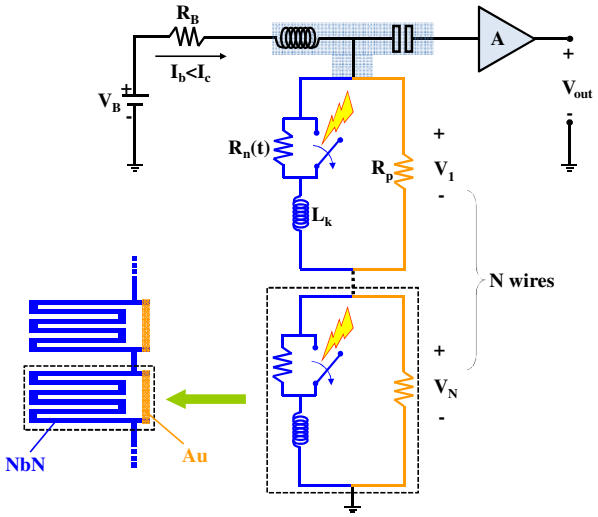

Fig. 1. Electrical circuit and layout schematics for the implementation of SND structures. The voltage source in series with a bias resistor provides the biasing of the detector through the DC arm of the bias-T. The RF arm is connected to the amplifier circuit. *N* nanowires, each with a resistor in parallel, are connected in series. The voltages produced by photon absorption in different sections are summed up in the output.

3. Simulation method

To assess the validity of our design, we perform an electrothermal simulation following the procedure in [22]. In this model, the heat equation is solved to obtain the spatial temperature distribution of the nanowire over time, which in principle determines which sections of a superconductive nanowire become resistive upon absorption of a single photon.

The heat flow Eq. (1) relates the heat generation (by Joule heating) and heat dissipation (by thermal conduction along the wire and through the substrate) to the rate of change of energy density in the nanowire.

$$J^2\rho + \kappa\frac{\partial^2 T}{\partial x^2} - \frac{\alpha}{d}\left(T - T_{sub}\right) = \frac{\partial\left(cT\right)}{\partial t}, \qquad (1)$$

In Eq. (1), $T(x,t)$ is the wire temperature, T_{sub} is the substrate temperature, J is the current density through the wire, ρ is the normal state resistivity of the superconducting film, κ is the thermal conductivity of the wire, α is the thermal boundary conductivity between nanowire and substrate, d is the nanowire thickness, and c is the specific heat per unit volume of the wire. The first term of Eq. (1), $J^2\rho$ represents Joule heating and couples the thermal equation to the electrical equations governing the circuit.

To solve Eq. (1) we consider the nanowire as a one dimensional structure and apply the finite difference method in MATLAB. At each time step, the thermal equation can be evaluated for a single wire (representing all the firing branches in series) to find the temperature and determine the state of each segment in the wire. A segment is considered resistive, if its current is higher than the critical current at the related temperature or its temperature exceeds the critical temperature, accordingly a non-zero value of electrical resistivity is assigned to it. The total resistance is then calculated as the sum of the resistances of each segment and used in the next step. Assuming that wires are identical within few percents, as normally achieved in high performance SSPDs, we can, without loss of

#157785 - $15.00 USD Received 9 Nov 2011; revised 16 Jan 2012; accepted 7 Feb 2012; published 14 Feb 2012

generality, use an electrical equivalent circuit model where all firing (unfiring) sections are lumped together (Fig. 2), simplifying the electrical circuit. A single thermal equation can be solved for a firing branch (representing all the detecting branches), providing the resistance value $R_n(t)$ which is then used to solve the circuit.

The simulation is initiated with the photon absorption at the center of a (firing) wire which forms a small resistive segment across it (the hotspot thermalization length, L_{th} [22]). Since the wire is biased close to its critical current, a resistive segment produces a source of Joule heating which is dissipated through the substrate and along the wire, heating up the wire and causing the resistive domain to grow further. Meanwhile, the corresponding normal resistance causes the bias current from the wire to be repelled to its parallel resistor (and partially to the load), creating a negative feedback to ensure self-resetting of the detector to superconducting state after each photon absorption event.

We consider SND structures made of d = 4.1nm thick, w = 100nm wide NbN nanowires on a GaAs substrate, folded in a meander with f = 50% filling factor. Two cases with N = 10, 4μm-long detecting sections and N = 100, 40μm-long detecting sections in series are considered giving square total detection area of 4μm x 4μm and 40μm x 40μm, respectively. Based on the experimental current-voltage characteristics of a typical NbN SSPD on GaAs [17], the macroscopic thermal properties of NbN nanowire required for solving the thermal equation are extracted. All the wires are assumed identical with critical temperature T_c = 10.5K, and critical current I_c = 22μA at the base temperature of T_{sub} = 2K, with the kinetic inductance L_k = 90pH/□. The normal region resistivity is ρ = 3μΩm, α = 1.92x10^{5}W/Ωm at 2K, and L_{th} = 25nm. The value of the parallel resistor to each detection section is chosen to be R_p = 80Ω, avoiding any latching or unwanted oscillation [23].

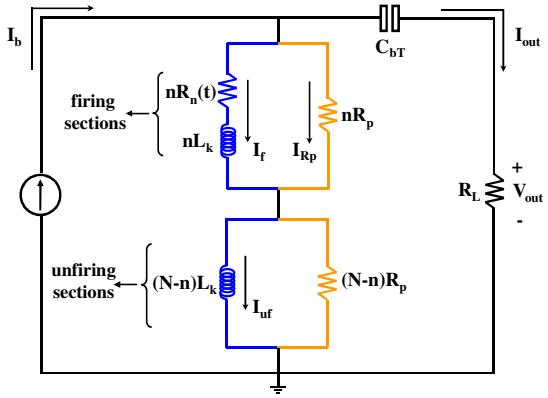

Fig. 2. Equivalent circuit model for the firing and unfiring sections of the SND. The DC port of the bias-T is modeled as a constant current source I_b and the AC port is modeled as a capacitor C_{bT} (20nF).

In the following, we consider two cases for the readout: A standard R_L = 50Ω load via a coaxial cable and room-temperature amplifier, and a high impedance (1MΩ) readout that can be achieved for instance by a high impedance cryogenic preamplifier mounted close to the detector. The latter paves the way for realization of scalable SNDs which provide a large number of detecting elements.

4. SND electrothermal responses

Using the electrothermal model, we are able to simulate the temperature change and the growth of the resistive region along the wire after photon absorption. Figure 3(a) shows the temporal evolution of temperature along a switching wire in an SND with N = 10 sections with the load impedance of R_L = 50Ω (R_L = 1MΩ gives identical results). Photon absorption at time t = 0 and the subsequent Joule heating lead to the growth of the initial hotspot,

#157785 - $15.00 USD Received 9 Nov 2011; revised 16 Jan 2012; accepted 7 Feb 2012; published 14 Feb 2012

forming a time-variable resistor, as shown in Fig. 3(b). As long as the temperature is increasing, more regions become resistive, leading to a maximum resistance of $R_n \approx 320\Omega$. This resistive region starts to shrink as the bias current is diverted to R_p, and finally disappears in ~50ps. Figure 3(c) and d show the corresponding temperature map and $R_n(t)$ for the case of an N = 100 sections SND, where the number of squares for each element (and consequently L_k) is 10 times larger. In this case, due to the larger kinetic inductance, the hotspot expands more before it cools down. This results in a normal state resistance of ~1.1kΩ which drops down to zero in ~110ps. We note that although the maximum temperature of the hotspot in both cases is still lower than T_c, the superconducting to normal transition occurs in the hot regions when the bias current exceeds the critical current, which strongly decreases as the temperature rises.

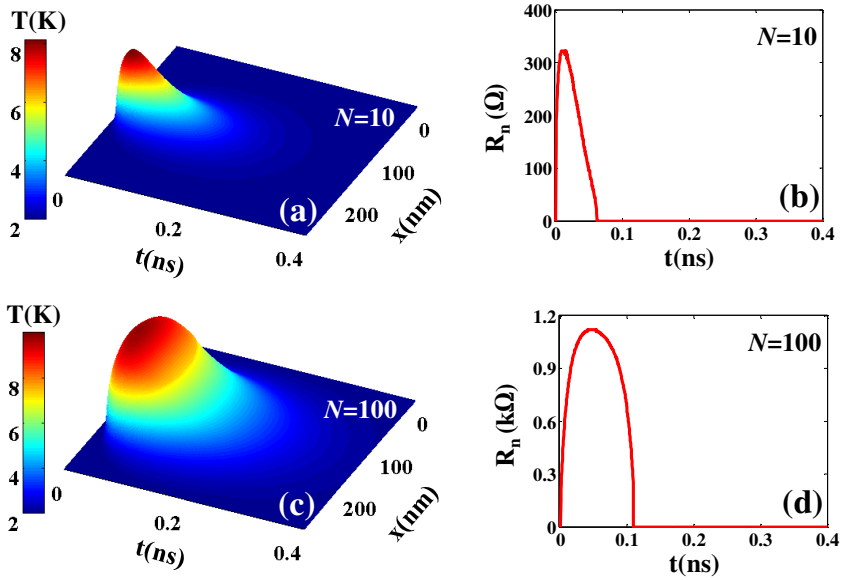

Fig. 3. Electro-thermal simulation for a firing section of an SND, biased with $I_b = 0.99I_c$, and R_L = 1MΩ. (a) Temperature map vs. time along the switching wire after photon detection in a N = 10 elements SND. (b) Time-dependent resistance for N = 10. (c) The same temperature map for N = 100. (d) Time-dependent resistance for N = 100.

The transient responses of an SND with N = 10 detection elements, when n = 1 to n = 10 photons are absorbed in distinct branches are investigated in Fig. 4. Figure 4(a), 4(b), and 4(c) illustrate the case for $R_L = 50\Omega$ readout. The transient current flowing through a firing and an unfiring branch of the SND are illustrated in Fig. 4(a), and 4(b) respectively. Initially, all the wires are superconducting, carrying a bias current $I_b = 0.99I_c$ with zero voltage drop across the branches. Photon absorption in the (firing) wire depletes it temporarily from most of its bias current (Fig. 4(a)). The depleted current is redistributed in part to the parallel resistor and in part to the load, producing voltage pulses across them. On the other hand, since a part of I_b is redistributed to the load, the total bias current going through the detector decrease. This brings about two undesirable effects. Firstly, it reduces the efficiency of all the wires, including the unfiring branches, effectively producing a dead time of few ns (Fig. 4(b)). Secondly, the kinetic inductances of the unfiring branches oppose to the change in the bias current by inducing a negative voltage. This reduces the total output voltage as compared to the ideal case.

#157785 - $15.00 USD Received 9 Nov 2011; revised 16 Jan 2012; accepted 7 Feb 2012; published 14 Feb 2012

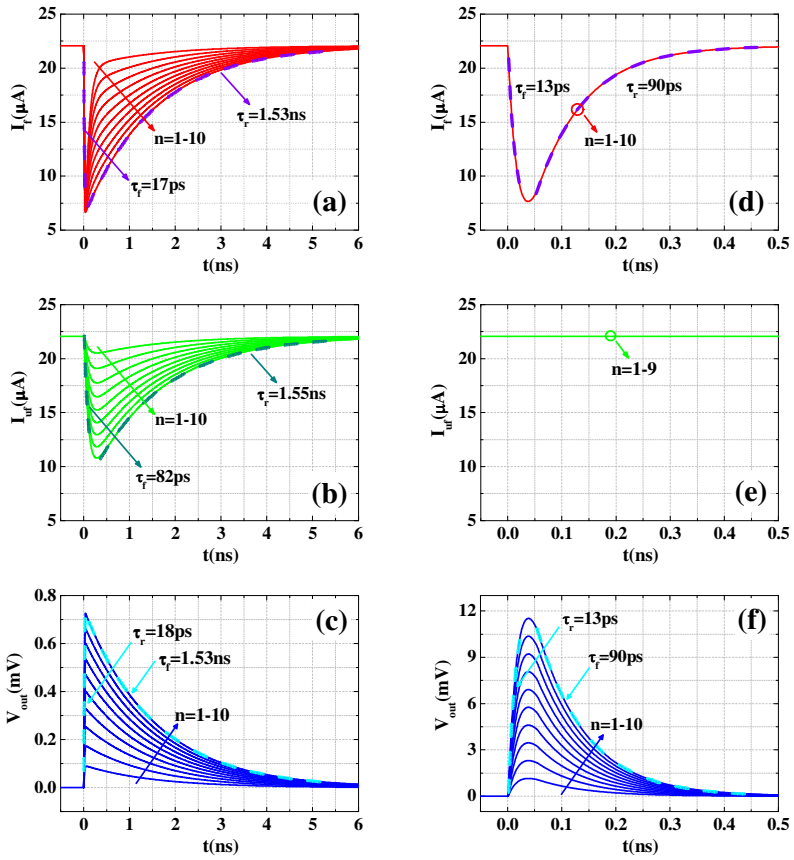

Fig. 4. Transient current flowing through the (a) firing, I_f and (b) unfiring, I_{uf} section of an SND with N = 10, R_L = 50Ω, I_b = 0.99Ic, R_p = 80Ω after absorption of n = 1-10 photons. (c) Corresponding output voltage V_{out}. Transient current (d) I_f and (e) I_{uf} with the ideal 1MΩ load readout, which are independent of the number of absorbed photons. The large load impedance decouples firing and unfiring sections. (f) The related output voltage with R_L = 1MΩ. The dashed lines are exponential fits to the rise/fall times, as explained in section 6.

Figure 4(c) shows the related output voltage transients. The peak output voltage is nearly proportional to the number of switching wires, as it will be shown below. Due to the negative voltage produced across the unfiring branches, the voltage formed across each firing branch cannot be fully measured at the output, so the output voltage is much smaller than sum of the voltages across the firing branches. As shown in Fig. 4(c), the voltage step between n and n + 1 in this case is in the order of ~80-90μV, much smaller than the ideal value of ~1mV which is produced by the current flowing through the parallel resistor R_p. We note that the typical minimum voltage pulse which can be correctly amplified and counted using a room temperature amplifier connected to the device via coaxial cable is in the range of 30-40μV in our setup, which means that, with N = 10, signal to noise ratio (SNR) is >2. Increasing the number of wires beyond 10 results in smaller voltage step increments and requires cryogenic readout. We show below how implementing a high impedance readout solves this issue.

One advantage of the series configuration over the parallel is that the current of the unfiring sections decreases, instead of increasing, due to current redistribution. Therefore, in the SND current redistribution only reduces the output voltage and produces a dead time (of the order of few ns), while in the PND it causes the bias current of the unfiring section to exceed the critical current, which results in the switching of the unfiring wire and a false

#157785 - $15.00 USD Received 9 Nov 2011; revised 16 Jan 2012; accepted 7 Feb 2012; published 14 Feb 2012

detection. This issue gets worse when the number of detecting elements in the PND is increased. In contrast, an SND, even with a large number of wires and hence a high dynamic range, can be biased very close to its I_c, getting benefit from its maximum QE.

Figure 4(d)–4(f) show the transient responses of the same SND with a high impedance readout of R_L = 1MΩ. In this case, the current redistribution problem is not present. The current transient in the firing branches does not depend on the number of switching wires, and is entirely diverted to parallel resistor. The current of the unfiring section also remains unchanged, i.e. $I_{uf} = I_b$ (Fig. 4(e)). Therefore, the voltage developed across a section after each photon detection event is accurately measured across the load and the voltage of the unfiring branch remains zero. In other words, the detection sections are decoupled from each other, which is highly favorable for a PNR detector. Furthermore, the higher voltage levels produced at the high impedance load are substantially easier to read out (Fig. 4(f)). This becomes more important in discriminating n and $n + 1$ states, particularly when dealing with large dynamic ranges.

As an example, to show how a high input impedance load allows scaling to much larger numbers of wires, we present the case of N = 100 wires, in an active area of 40μm x 40μm. Figure 5(a) shows the transient current flowing through the firing branch (I_f), its parallel resistor (I_{Rp}), the unfiring branch (I_{uf}), and the load resistor (I_{out}) after n = 1-100 photon detection event in an SND with N = 100, I_b = 0.99I_c, R_p = 80Ω, and assuming R_L = 1MΩ. It is clearly shown that all the current repelled from the switching wire flows only into the parallel resistor ($I_{Rp} = I_b - I_f$), and no current goes through the load (I_{out} = 0), therefore the bias current remains unchanged in the unfiring branches ($I_{uf} = I_b$). In Fig. 5(b), the related output voltage for n = 1, 2 and 3 are shown emphasizing the relatively large voltage step size of ~1.2mV.

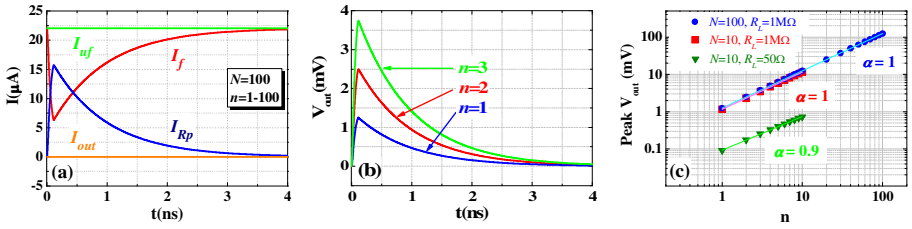

Fig. 5. Transient response of an SND with N = 100, I_b = 0.99I_c, R_p = 80Ω, and R_L = 1MΩ. (a) Current flowing through the firing I_f, and unfiring I_{uf}, sections, the parallel resistor I_{Rp}, and the load I_{out}. (b) Output voltage of the SND when n = 1,2,3 photons are absorbed. (c) Peak output voltages as a function of the number of absorbed photons together with a power-law fit (solid lines) plotted in log-log scale as $V_{out} = An^{\alpha}$. For the case of the high impedance load (1MΩ), α = 1 both for N = 10 and N = 100, (red squares and blue circles, respectively). The response is very close to linear (α = 0.9) even with the 50Ω load (green triangles).

Figure 5(c) compares the peak output voltages versus the number of switching wires in log-log scale, in SNDs of N = 10 and N = 100, with 50Ω and high impedance readout for N = 10 and only high impedance readout for N = 100. Although the conventional 50Ω readout produces a response close to linear, the signal level is reduced a lot, due to the fact that not all the voltage produced across the parallel resistors is read at the 50Ω load. For the high impedance load, however, perfect linearity as well as easy voltage readout is achieved. We note that the slightly larger output voltage and slower response for the N = 100 case is due the larger wire length and kinetic inductance used for the N = 100 design.

5. Dynamic characteristics of the SND

In order to provide further insight into the dynamics of the SND, the electrical circuit can be simplified according to the knowledge gained from the electrothermal model. The nonlinear resistor $R_n(t)$ can be modeled as a switch, initially open to a large resistance (normal resistance of the nanowire), which drops to zero in a step-like manner. Discarding the

#157785 - $15.00 USD Received 9 Nov 2011; revised 16 Jan 2012; accepted 7 Feb 2012; published 14 Feb 2012

negligible effect of the bias-T capacitance, the two inductive elements (related to the firing and unfiring branches) in the equivalent circuit of Fig. 2 suggest that the circuit can be described by a 2nd order differential equation, therefore the transient responses include two time constants. In Fig. 6 the equivalent circuits used to estimate the time constants for each inductive element of the circuit are shown. Figure 6(a) and 6(b) show the equivalent circuits seen by the inductances of the firing and unfiring inductors, respectively, when the nanowire is in the resistive state. The time constants τ_1 and τ_2 associated to the firing and unfiring sections determine the pulse rise time, and it is easily seen that τ_1 is always smaller than τ_2, because of the relatively large resistance of the wire in the normal state. When the nanowire switches back to the superconducting state, the inductances can be lumped together and the problem is simplified to a single *RL* circuit with a time constant of τ_3 as shown in Fig. 6(c), which determines the pulse decay time.

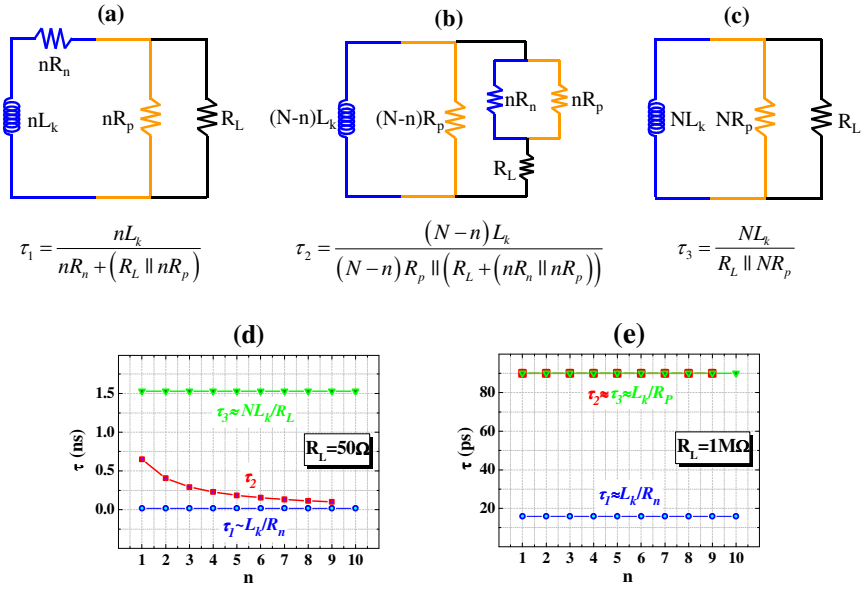

Fig. 6. Equivalent circuits used to extract the time constants corresponding to the (a) inductances of the firing branches, (b) inductances of the unfiring branches, and (c) the total inductance after the wires have switched back to the superconducting state. (d), (e) The calculated time constants of the N = 10 elements SND with R_L = 50Ω and R_L = 1MΩ, respectively. Increasing R_L improves the response time dramatically, without causing latching.

In Fig. 6(d) the three different time constants τ_1-τ_3, calculated for the SND with N = 10 elements and R_L = 50Ω, are plotted as a function of n. It is seen that τ_1 and τ_3 are almost independent of n. For nR_n>(R_L||nR_p), τ_1 tends to $\tau_1 \approx L_k / R_n$ which is in the range of 20ps for this case while $\tau_3 \approx NL_k/R_L \approx$1.5ns. We note that our calculations do not take into account the hotspot relaxation dynamics which will become significant for rise times in the 20ps range. It is noteworthy to mention that τ_1 is more than N times smaller than the one of a standard SSPD having the same active area (= L_k /R_L), while the recovery time of the SND is exactly the same as a standard SSPD of the same size (= NL_k/R_L). In Fig. 6(e) the time constants related to the high impedance load of R_L = 1MΩ are plotted. It is clear that a large value of R_L results in $\tau_1 \approx L_k/(R_n + R_p) \approx L_k/R_n$ and $\tau_2 \approx \tau_3 \approx L_k/R_p$ which means that the recovery time is improved at least by a factor of N. This implies that as far as R_p is chosen so that it avoids latching, increasing R_L has no effect on latching but favors the SND with a much faster response time. The SND can therefore also be used as a large area single-photon detector with ultrahigh counting rates.

#157785 - $15.00 USD Received 9 Nov 2011; revised 16 Jan 2012; accepted 7 Feb 2012; published 14 Feb 2012

To verify the estimated transient dynamics, in Fig. 4 the transient responses for some special cases are fitted with exponential functions (dashed lines), which all correspond very well with the expected time constants τ_1 and τ_3, given in the equations of Fig. 6. We can conclude that for the $N = 10$ elements SND, the maximum repetition range can reach nearly 200MHz with a traditional readout, while with a high impedance readout it can exceed 2GHz.

6. SND response with realistic high-impedance readout

In the preceding sections, the advantages of using a preamplifier with high input impedance were shown. However, it is worth mentioning that the frequency response of such preamplifier, and particularly its input capacitance, might impose some limits on the performance of the detector. Therefore the SND design must be optimised taking into account the actual preamplifier characteristics. For instance, using a commercially available HEMT in the common source configuration in the cryogenic preamplifier stage with the total input capacitance of $C = 180$fF for reading out an SND with $N = 10$ sections, requires a change in the value of the parallel and load resistors to $R_p = 40\Omega$ and $R_L = 10\text{k}\Omega$, respectively, to avoid latching. For an SND with $N = 100$ sections with $R_p = 40\Omega$, the load resistance can be kept as $R_L = 1\text{M}\Omega$. The output voltages considering the added parallel capacitance at $I_b = 0.99I_c$ for the case of n = 1-10 detected photons are shown in Fig. 7, with the insets showing the linearity of the output voltages versus the number of detected photons. It is seen that although lowering R_p and R_L decreases the signal amplitude, the effect on the linearity is marginal and both output amplitude and linearity are still much better than the case of 50Ω readout.

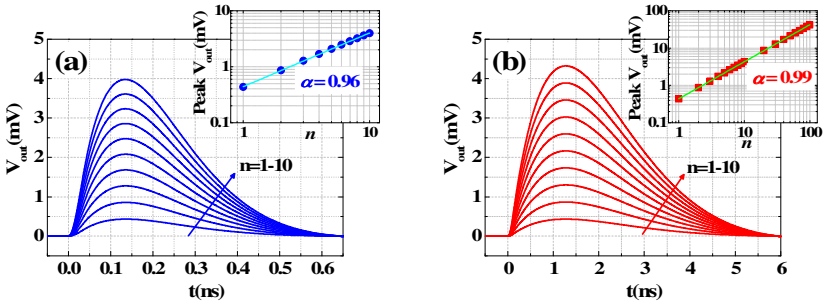

Fig. 7. Output voltage of an SND with N series section each connected in parallel to $R_p = 40\Omega$ and biased at $I_b = 0.99I_c$, considering the effect of $C = 180$fF input capacitor in parallel to the load resistor. (a) $N = 10$, and $R_L = 10\text{k}\Omega$ when $n = 1,2,\ldots,10$ photons are detected. The inset shows the linearity of the peak output voltages as a function of the number of detected photons together with a power-law fit (solid line) plotted in log-log scale as $V_{out} = An^{\alpha}$ where $\alpha = 0.96$ (b) $N = 100$, and $R_L = 1\text{M}\Omega$. The inset shows the power-law fit of n = 1-100 detected photons with excellent linearity of $\alpha = 0.99$.

In this case, although the rise time is affected by the added RC time constant, the dynamic characteristic for the recovery time (fall time) is still dominated by the time constant related to the kinetic inductance, i.e. $\tau \approx L_k/R_p$. Note that the longer fall times in Fig. 7 compared to Figs. 4 and 5 stem from the fact that in the circuit with $C = 180$fF in parallel to R_L, a smaller R_p (40Ω) is chosen in order to avoid latching or unwanted oscillations.

7. Limitations of the fidelity in an SND

The considerations above only pertain to the linearity of the output voltage as a function of the number of firing sections. In a spatially-multiplexed detector, such as the SND, the finite number of sections and imperfect efficiency can further limit an accurate measurement of the photon number. In order to discuss these limitations, it is useful to distinguish between two classes of applications for which a PNR can be used. On one hand, in photonic quantum information processing, the number of photons produced in a setup (e.g. a probabilistic quantum gate) must be accurately measured. In this case, the detector is best characterized

#157785 - $15.00 USD Received 9 Nov 2011; revised 16 Jan 2012; accepted 7 Feb 2012; published 14 Feb 2012

through the associated positive-operator-valued-measure (POVM) matrices [24], which boil down to the probabilities $P(m|n)$ of measuring m photons when n are incident. Here, we take the probability $P(n|n)$ of correctly measuring n incident photons as a measure of fidelity. In order to maximize the probability of detecting all photons in an optical pulse, it is necessary that the number N of detection elements is much larger than n, so that the probability that two or more photons are absorbed in the same detector is small. On the other hand, each detecting element may have a non-unity QE, which imposes another limitation to the fidelity of photon state detection, resulting in an underestimation of the number of incident photons. As shown in [8], when n photons are evenly distributed to N output modes ($n \le N$), and at each output mode there is a detector with quantum efficiency QE = η, the probability of detecting all n photons is given by: $P_\eta^N(n|n) = (\eta/N)^n N!/(N-n)!$. In Fig. 8(a), $P_\eta^N(n|n)$ is plotted for n = 1-10 photons, with a N = 100 element-SND, assuming three cases with QE values of 1, 0.9 and 0.8 for all the detecting elements. As it was previously shown [8,11] having high QE is crucial, especially when detection of large photon states is required. The integration of nanowires with microcavities [20] and waveguides [21] has already resulted in QE values in the 80-90% range. The fidelity of SND is similar to other PNR detectors based on multiplexing techniques [8–12]. While approaches based on the direct measurement of the total pulse energy, such as the TES [5], do not suffer from the limited number of elements, the high speed and comparatively high operating temperature make the SND a unique candidate for quantum photonics applications, especially for PNR detection in the telecom wavelength range.

Another application of the SND is to work as a very sensitive linear optical detector of classical light, determining the average number of photons in a weak coherent optical source, for example in ultra-long distance optical communication or optical time domain reflectometry. Also in this case a possible limitation is represented by the finite probability that photons are absorbed in the same nanowire, leading to an underestimation of the average number of incident photons. In contrast, the non-unity QE does not affect the SND performance, apart from a reduction in sensitivity, since a Poissonian photon distribution remains Poissonian under the influence of linear loss, and the average detected photon number scales simply as the QE. The symbols in Fig. 8(b) show the average number of detected photons $\langle n_{det} \rangle$ as a function of the average number of incident photons per pulse $\langle n_{inc} \rangle$ assuming a Poissonian source, for an SND with N = 100 elements and QE = 1, calculated as described in [8]. The comparison of the results with the unity-slope line (in light blue) reveals that the linearity is conserved in the limit $n \ll N$, with increasing saturation as n approaches N. However, the deviation from a linear slope is quite acceptable even for $n \sim N/2$.

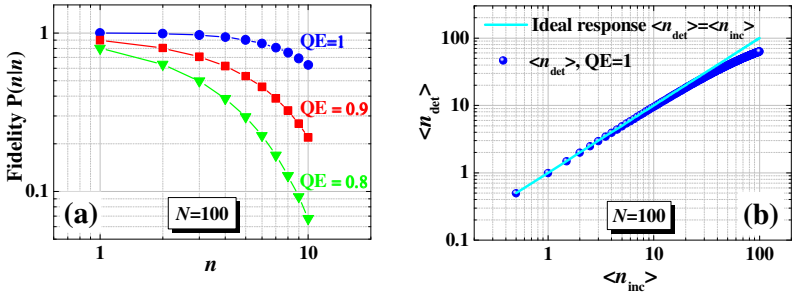

Fig. 8. (a) Probability of detecting n = 1-10 photons when n = 1-10photons hit the SND with N = 100 detecting elements, with different values of QE = 0.8, 0.9, and 1. (b) Calculated average number of detected photons $\langle n_{det} \rangle$ as a function of the average number of incident photons $\langle n_{inc} \rangle$, evenly distributed to N = 100 detecting sections of the SND with unity QE (blue circles), compared with ideal response, the light blue line with slope = 1.

#157785 - $15.00 USD Received 9 Nov 2011; revised 16 Jan 2012; accepted 7 Feb 2012; published 14 Feb 2012

8. Conclusion

In conclusion, we have proposed a photon number resolving detector based on superconducting nanowires which is a promising candidate to fill the existing gap between the single photon and the linear detection regimes at telecom wavelengths. The combination of spatial multiplexing over a large number of nanowires in series and current discharging on the parallel resistors allows accurate voltage readout and circumvents the problems inherent to other wire connections. In combination with a high impedance load (e.g. a high input impedance cryogenic preamplifier stage mounted close to the device), a large array of series nanowires may allow photon number measurements in the range from one to several tens of photons with high fidelity and repetition rates in the hundreds of MHz range.

Acknowledgments

We would like to thank F. Marsili and E.J.G. Janssen for helpful discussions in the early stages of this work and F. Mattioli, A. Gaggero and R. Leoni for useful discussions on fabrication feasibility. This work is supported by the Dutch Technology Foundation STW, applied science division of NWO, the Technology Program of the Ministry of Economic Affairs under project No. 10380, the Dutch HTMS program and the European Commission through FP7 Q-ESSENCE (Contract No. 248095).

#157785 - $15.00 USD Received 9 Nov 2011; revised 16 Jan 2012; accepted 7 Feb 2012; published 14 Feb 2012